The $(2n+1)$th-order off-resonant spectroscopy from the $(n+1)$th-order anharmonicities of molecular vibrational modes in the condensed phase

K. Okumura and Y. Tanimura
Division of Theoretical Studies, Institute for Molecular Science, Myodaiji, Okazaki, Aichi 444, Japan

(Received 5 August 1996; accepted 23 October 1996)

Assuming that the polarizability is a linear function of the nuclear coordinate, i.e., $\alpha(q)=\alpha_0+\alpha_1 q$, we obtain analytical expressions of the $(2n+1)$th-order signals and show that the leading order of the signals $(n>1)$ is proportional to g_{n+1}, where g_{n+1} is the coefficient of the anharmonic potential $V(q)=g_3q^3/3!+g_4q^4/4!+\cdots$. In other words, detection of the $(2n+1)$th-order signal implies the direct observation of the $(n+1)$th-order anharmonicity within the approximation. Based on this fact we discuss a possibility to detect the $(n+1)$th-order anharmonicity directly from the $(2n+1)$th-order experiment. Calculations are made by using novel Feynman rules for the nonequilibrium multitime correlation functions relevant to the higher-order off-resonant spectroscopy. The rules have been developed by the authors and are presented compactly in this paper. With the help of a conventional double-sided Feynman diagram, we draw physical pictures of higher-order off-resonant optical processes. Representative calculations for $CHCl_3$ of the fifth-, seventh-, and ninth-order optical processes are presented and discussed. © *1997 American Institute of Physics.*
[S0021-9606(97)50805-1]

I. INTRODUCTION

Dynamics of intra- and intermolecular vibrational modes in the condensed phase play a crucial role in various chemical reactions. The extensive development of ultrafast pulse lasers has made it possible to measure spectroscopy of the low-frequency vibrational modes in real time. The time-domain third-order techniques, such as femtosecond optical Kerr effect (OKE),[1,2] and impulsive stimulated Raman scattering (ISS),[3] have directly detected dephasing of the low-frequency modes of liquids.

It is natural that experiments of higher nonlinear response are more selective. One of the examples is Raman-echo experiments[4–7] related to the seventh order. Another is the two-dimensional off-resonant experiment related to the fifth-order nonlinearity.[8–14] These experiments were carried out to separate the inhomogeneous and homogeneous dephasing. In our previous paper[15] we showed that off-resonant fifth-order optical processes can also be used to separate effects of third-order anharmonicity $(g_3q^3/3!)$ of vibrational modes from the other effects, such as nonlinear coordinate dependence of polarization. In the present paper, we generalize our previous study of the fifth-order optical process to the $(2n+1)$th order and show that $(2n+1)$th-order off-resonant spectroscopy is useful to study the $(n+1)$th-order anharmonicity g_{n+1}.

We employ the multimode (anharmonic) Brownian oscillator model (for a harmonic Brownian oscillator model, see, for example, Refs. 16 and 17) to incorporate the intra- and intermolecular modes in the condensed phase. The $(2n+1)$th-order off-resonant signal can be expressed by the multicommutator of the $(n+1)$-time correlation function of the polarizability. For example, the signal of the third-order $(n=1)$ experiment such as ISS and OKE can be directly related to the two-time correlation function, $R^{(3)}\propto\langle[\alpha(t),\alpha(0)]\rangle$. To calculate such multitime correlation functions for an anharmonic system, we use the nonequilibrium generating functional obtained in Ref. 18.

If we assume polarization is a linear function of the nuclear coordinate, i.e., $\alpha=\alpha_0+\alpha_1 q$, the response functions are expressed as the multitime correlation function of coordinates, $\langle[q(t),q]\rangle$,$\langle[q(t),q(t')],q]\rangle$, etc. Here, the anharmonicity plays a significant role, since correlation functions of the multicommutator of coordinate higher than the third order vanish for the harmonic potential or in the (harmonic) Brownian particle system. In the real world, the anharmonicity often becomes important. For example, the low-frequency vibrational modes of water were found to have weak anharmonicity.[19]

We incorporate anharmonicity[20] into the Brownian motion theory through Feynman diagrammatic technique, as done in our previous works.[15,18,21] In the present article, we refine our Feynman diagrammatic technique in the form which we call the three-step Feynman rule. The conventional Feynman diagram technique (for finite temperature or for zero temperature) has only two steps: (1) draw Feynman diagrams and (2) obtain analytical expressions from the diagrams. Here, we deal with the nonequilibrium expectation, and the diagrammatic technique can be described by three steps: (1) draw *simplified* Feynman diagrams; (2) draw *specified* Feynman diagrams; and (3) obtain analytical expression from the specified diagram.

In general, a single graph in this three-step method corresponds to a sum of many double-sided Feynman diagrams.[17] Thus, calculation is simpler in the three-step method. The physical picture from the three-step method is, however, not as clear as that from the double-sided Feynman diagrams; each double-sided Feynman diagram has one-to-one correspondence to the Liouville space path.[17] Therefore, we use the double-sided technique complementary in the present paper.

In Sec. II, we specify our model for the off-resonant experiment and define multicommutator correlation functions which can be directly measured by the experiment. In Sec. III, we give analytical expressions of the response functions relevant to $(2n+1)$th-order experiments by using the three-step method, which is summarized as rules A, B, and C, with some examples in Appendix A. In Sec. IV, the conventional double-sided diagrams (corresponding to the analytical expression obtained in Sec. III) are presented to understand profiles of signals from physical picture. In Sec. V, we take parameters from the OKE experiment on chloroform,[2] carry out numerical calculations, and give physical interpretations of the results. In the final section, we discuss limitations and possible extentions of the present work.

II. FEYNMAN RULE FOR THE $(2n+1)$TH CORRELATION FUNCTION

We consider a molecular system in the condensed phase which is subject to electronically off-resonant pulses. The off-resonant pulses can selectively probe only the electronic ground state dynamics. The effective Hamiltonian is given by

$$H_{\mathrm{eff}}=\hat{H}(p,q)-\hat{P}E(\mathbf{r},t),\tag{2.1}$$

where p and q stand for the momentum and coordinate of the nuclear degrees of freedom, respectively. In this experiment, the permanent electronic dipole does not play a role. Instead only the induced dipole

$$\hat{P}=\hat{\alpha}E(t)\tag{2.2}$$

is probed, where $\hat{\alpha}$ is the polarizability. In the following we consider the case in which the nuclear motion is described by a single mode. Generalization to the multimode case is straightforward (see Ref. 15). We consider the ground state Hamiltonian coupled to an environment in the form

$$\hat{H}(p,q)=\frac{p^2}{2m}+\frac{m\omega^2}{2}q^2+V(q)+\sum_{i=1}^{N}\left[\frac{p_i^2}{2m_i}+\frac{m_i\omega_i^2}{2}\left(q_i-\frac{c_iq}{m_i\omega_i^2}\right)^2\right].\tag{2.3}$$

The corresponding classical equation of motion of q for this Hamiltonian has the memory friction $\gamma(t)$, which is completely specified by the bath parameters (c_i,m_i,ω_i). All information about the bath which is set by the parameters (c_i,m_i,ω_i) is concentrated on the quantity $\gamma(t)$ even in the quantum treatment. Thus, we can parameterize the theory in terms of $\gamma(t)$ instead of specifying all the values (c_i,m_i,ω_i). In the following, we employ the Ohmic model assuming $\gamma(t)=\gamma\delta(t)$ where γ is a constant. This choice is allowed only when we let $N\to\infty$.

The variation of the polarizability with the nuclear coordinate is assumed to be

$$\hat{\alpha}=\alpha_0+\alpha_1q+\frac{1}{2!}\alpha_2q^2+\cdots=\sum_{i=0}\frac{1}{i!}\alpha_iq^i\equiv\sum_{i=0}\alpha_i(q).\tag{2.4}$$

The anharmonicity of the potential is given by

$$V(q)=\frac{1}{3!}g_3q^3+\frac{1}{4!}g_4q^4+\cdots=\sum_{i=3}\frac{1}{i!}g_iq^i\equiv\sum_{i=3}V_i(q).\tag{2.5}$$

The $(2n+1)$th-order off-resonant signal is expressed as[8,15,17]

$$I^{(2n+1)}(T_1,T_2,\ldots,T_n)=|R^{(2n+1)}(T_1,T_2,\ldots,T_n)|^2.\tag{2.6}$$

The response functions are defined through the multicommutators:

$$R^{(3)}(T_1)=\frac{i}{\hbar}\langle[\alpha(T_1),\alpha(0)]\rangle,\tag{2.7}$$

$$R^{(5)}(T_1,T_2)=\left(\frac{i}{\hbar}\right)^2\langle[[\alpha(T_1+T_2),\alpha(T_1)],\alpha(0)]\rangle,\tag{2.8}$$

$$\vdots\tag{2.9}$$

$$R^{(2n+1)}(T_1,T_2,\cdots,T_n)\tag{2.10}$$

$$=\left(\frac{i}{\hbar}\right)^n\langle[\cdots[\alpha(T_1+T_2+\cdots+T_n),\alpha(T_1+\cdots+T_{n-1})],\cdots\alpha(T_1)],\alpha(0)]\rangle,\tag{2.11}$$

where $\alpha(t)$ is the Heisenberg operator defined by the Hamiltonian $\hat{H}(p,q)$ in (2.3), or

$$\alpha(t)=e^{i\hat{H}t/\hbar}\hat{\alpha}e^{-i\hat{H}t/\hbar},\tag{2.12}$$

and the expectation implies

$$\langle\cdots\rangle=\mathrm{Tr}[e^{-\beta\hat{H}}\cdots]/\mathrm{Tr}[e^{-\beta\hat{H}}].\tag{2.13}$$

The response functions can be expressed by the sum of either of the two types of connected Feynman diagram:

$$R^{(2n+1)}(T_1,T_2,\cdots,T_n)\tag{2.14}$$

$$=\sum[\text{topologically distinct simplified diagrams}]\tag{2.15}$$

$$=\sum[\text{topologically distinct specified diagrams}].\tag{2.16}$$

Here, the summation Σ implies the one over all possible diagrams. Detailed explanations are given in Appendices A and B with some examples. We have three types of *time* evolution operators, since we are calculating the expectation values in the nonequilibrium system. These three operators, the real time evolution operator of the ket $(e^{-i\hat{H}t/\hbar})$, that of the bra $(e^{i\hat{H}t/\hbar})$, and the imaginary time evolution operator $(e^{-\beta\hat{H}})$, are associated with the C_1-path, C_2-path, and

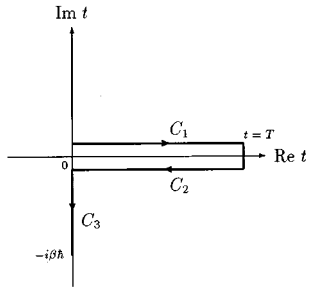

FIG. 1. The unified time-path $C=C_1+C_2+C_3$ on the complex t plane $(T\to\infty)$. C_1 and C_2 are along the real-time axis, whereas C_3 is on the imaginary axis.

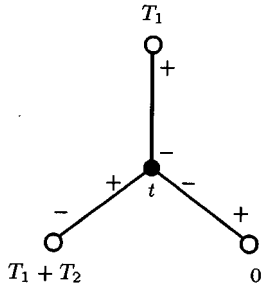

FIG. 2. The specified diagram for the leading order of $R^{(5)}$.

C_3-path, respectively, or with the unified time path $C=C_1+C_2+C_3$ (see Fig. 1). In the conventional case[22] where calculation of the expectation at the equilibrium is the main goal, only the imaginary time evolution operator, $e^{-\beta\hat{H}}$ (corresponding to the C_3-path), is required. Thus, the propagators appearing in the rule for the finite temperature always connect two points on C_3 (Matsubara Green functions). On the contrary, we have the three paths C_1, C_2, and C_3 in the present case of nonequilibrium expectation. Then the propagators in this case connect arbitrarily two points on the unified time path $C=C_1+C_2+C_3$. In other words, we have a propagator matrix $D^{ij}(i,j=1,2,3)$. For convenience, we take the linear combinations of the four independent elements, $D^{(-+)}$, $D^{(--)}$, $D^{(-3)}$, and $D^{(33)}$, of the 3×3 matrix. This is why we have to add the extra $(+,-,3)$ indices to the conventional Feynman diagrams to obtain the specified diagrams (see Appendix A).

By use of the simplified diagram, we can grasp the main contribution to the response function efficiently. Once a simplified diagram is written down, we can readily obtain the analytical expressions by way of the specified diagrams. Although calculations of the nonequilibrium expectation values are more complicated than those of the equilibrium ones, the three-step procedure presented here—obtaining simplified diagrams, and then specified diagrams to derive the analytical expressions—greatly simplifies calculations.

III. RESPONSE FUNCTIONS OF THE ANHARMONIC SYSTEM WITH THE LINEAR POLARIZABILITY

In the following, we employ the linear polarizability approximation in a sense that

$$\alpha=\alpha_0+\alpha_1 q,\neg \tag{3.1}$$

and calculate the response function relevant to the $(2n+1)$th-order experiment. In this model, the response function is given as

$$\begin{aligned}R^{(2n+1)}(T_1,T_2,\cdots,T_n)&=\left(\frac{i}{\hbar}\right)^n\alpha_1^{n+1}\langle[\cdots[q(T_1+\cdots+T_n),\\&\quad q(T_1+\cdots+T_{n-1})],\cdots,q(T_1)],q(0)]\rangle.\neg\end{aligned} \tag{3.2}$$

By use of the three-step procedure presented in Appendix A, the leading contribution is expressed as

$$\begin{aligned}R^{(5)}(T_1,T_2)&=-\left(\frac{i}{\hbar}\right)^3 g_3\alpha_1^3\int_{T_1}^{T_1+T_2}dtD^{(-+)}(T_1+T_2,t)\\&\quad\times D^{(-+)}(t,0)D^{(-+)}(t,T_1),\neg\end{aligned} \tag{3.3}$$

$$\begin{aligned}R^{(7)}(T_1,T_2,T_3)&=-\left(\frac{i}{\hbar}\right)^4 g_4\alpha_1^4\int_{T_1+T_2}^{T_1+T_2+T_3}dt\\&\quad\times D^{(-+)}(T_1+T_2+T_3,t)D^{(-+)}(t,0)\\&\quad\times D^{(-+)}(t,T_1)D^{(-+)}(t,T_1+T_2),\neg\end{aligned} \tag{3.4}$$

$$\begin{aligned}R^{(9)}(T_1,T_2,T_3,T_4)&=-\left(\frac{i}{\hbar}\right)^5 g_5\alpha_1^5\int_{T_1+T_2+T_3}^{T_1+T_2+T_3+T_4}dt\\&\quad\times D^{(-+)}(T_1+T_2+T_3+T_4,t)\\&\quad\times D^{(-+)}(t,0)D^{(-+)}(t,T_1)\\&\quad\times D^{(-+)}(t,T_1+T_2)\\&\quad\times D^{(-+)}(t,T_1+T_2+T_3),\neg\end{aligned} \tag{3.5}$$

$$\vdots$$

$$\begin{aligned}R^{(2n+1)}(T_1,\cdots,T_4)&=-\left(\frac{i}{\hbar}\right)^{n+1} g_{n+1}\alpha_1^{n+1}\int_{T_1+\cdots+T_{n-1}}^{T_1+\cdots+T_n}dt\\&\quad\times D^{(-+)}(T_1+\cdots+T_n,t)D^{(-+)}(t,0)D^{(-+)}(t,T_1)\cdots\\&\quad\times D^{(-+)}(t,T_1+\cdots+T_{n-1}).\neg\end{aligned} \tag{3.6}$$

The specified diagram for the fifth order is explicitly given in Fig. 2. The temperature-dependent propagators $D^{(-3)}$ and $D^{(33)}$ do not appear in the above leading order calculation; they play roles in higher-order contributions.

In the Ohmic case the propagator is calculated as

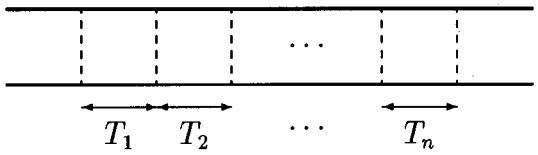

FIG. 3. The bare ladder diagram to create double-sided diagrams. The lower (upper) line stands for the real time evolution of the bra (ket) vector and corresponds to the $C_2^-(C_1^-)$ path.

$$D^{(-+)}(t,s)=\theta(t-s)\,\frac{\hbar}{im\,\zeta}\,e^{-\gamma(t-s)/2}\sin\,\zeta(t-s), \tag{3.7}$$

where

$$\zeta=\sqrt{\omega^2-\gamma^2/4}. \tag{3.8}$$

Note here that by using the formula for odd-n (and a similar formula for even-n),

$$\sin x_1\,\sin x_2\cdots\sin x_n$$
$$=\frac{(-1)^{(n-1)/2}}{2^{n-1}}\sum_{\epsilon_2=\pm1}\sum_{\epsilon_3=\pm1}\cdots\sum_{\epsilon_n=\pm1}(-1)^{\epsilon_2+\epsilon_3+\cdots+\epsilon_n}$$
$$\times\sin(x_1+\epsilon_2x_2+\epsilon_nx_3+\cdots+\epsilon_nx_n), \tag{3.9}$$

the integrations in Eqs. 3.3–3.6 can be readily performed. We use the result of this integration for the numerical calculations in Sec. V.

We stress here that the leading contribution is proportional to g_{n+1} and thus the detection of the nonzero $I^{(2n+1)}$ signal implies the direct observation of the $(n+1)$th anharmonicity within the linear polarization approximation.

As seen from Eqs. 3.3–3.6, the range of the integration is from $T_1+\cdots+T_{n-1}$ to $T_1+\cdots+T_n$, namely, the time integration is done for the period T_n, which indicates that the signal is caused by the anharmonic interaction *during this last period* T_n and thus becomes zero for $T_n=0$.

IV. DOUBLE-SIDED FEYNMAN DIAGRAM AND PHYSICAL PICTURE

Although the three-step Feynman rule simplifies calculations considerably, the physical picture of the diagram appearing in the three-step technique may be less clear than the double-sided Feynman diagram.[17] In this section, we illustrate a physical picture of signals from nonlinear optical processes by using the double-sided Feynman diagrams. Although the double-sided Feynman diagrams may be well-known in this field, to clarify our notations, in Appendix C we give explicit rules to draw the double-sided Feynman diagrams of the leading order contributions to the $(2n+1)$th-order response function (see Figs. 3 and 4).

Figure 4 shows a heuristic case where the vibrational mode of the electronic ground state is described by only two levels g_0 and g_1. We have $(n+1)$ black circles (laser interactions) and a cross (anharmonic interaction) on the base diagram. (If one considers higher-order correction of anharmonicity, one has more crosses.) In general, we have $2^{n+1}\times2(n+2)$ topologically different diagrams at the leading order. Note here that we have $2(n+2)$ distinct segments of the ladder: $2n$ segments corresponding to the period $T_1,\cdots,T_n$ and the remaining four segments to both ends of the ladder.[23] The three-step Feynman rule employed in the previous section does not require us to take care each of these large number of double-sided diagrams separately. Instead we have only to deal with fewer (non-double-sided) diagrams, although physical pictures from these diagrams may be less transparent than those from the double-sided ones. Therefore, we examine physical pictures with help of the double-sided diagrams.

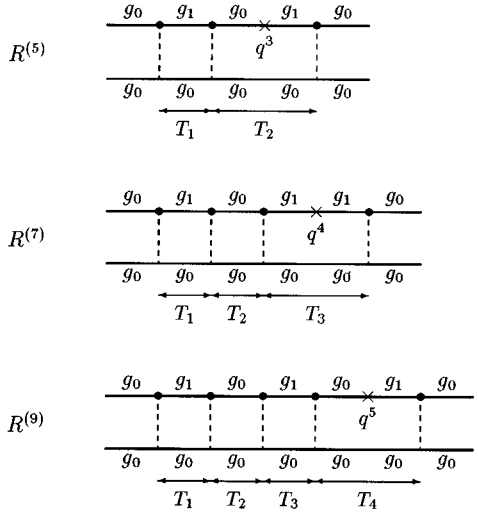

FIG. 4. Examples of the double-sided Feynman diagram for $R^{(5)}$, $R^{(7)}$, and $R^{(9)}$ for the system with only two vibrational levels g_0 and g_1. The black circle stands for the interaction with a pair of pulses, while the cross represents the anharmonic interaction. There are $2^3\times2\times4$ diagrams (including the one in the above) for $R^{(5)}$. The other $2^3\times2\times4-1$ diagrams can be obtained by moving the black circles up or down and moving the cross to another time segment. However, the diagrams which do not have the cross at the last period T_2 all cancel with each other (see text).

Results (3.3)–(3.6) obtained by the three-step method suggest that the double-sided diagrams which contribute to them are only the ones having the cross either on the two segments corresponding to the last period T_n. Note that the time integrations in our results (3.3)–(3.6) originate from the anharmonic interaction (the cross) and the range of the integrations are equal to T_n (from $T_1+\cdots+T_{n-1}$ to $T_1+\cdots+T_n$). All of the other double-sided diagrams [$2^{n+1}\times2(n+2)-2^{n+1}\times2$ in number] are exactly canceled out. This fact suggests that the signal becomes weak when the last period T_n is reduced and we expect a slow rise of the signals as a function of T_n.

To illustrate the physical picture more clearly, we restrict ourselves to the system whose electronic ground state is described by the two vibrational levels g_0 and g_1. The system is assumed to be initially in the g_0 state. One of the double-sided diagrams for the fifth, seventh, and ninth response functions is depicted in Fig. 4. We shall call the states denoted by $|g_0\rangle\langle g_0|$ and $|g_1\rangle\langle g_1|$ the vibrational population states, and $|g_0\rangle\langle g_1|$ and $|g_1\rangle\langle g_0|$ the vibrational coherence states.

TABLE I. States during each period T_i in the signal for the (vibrational) two-level system: the abbreviations coh. and pop. imply the coherence and the population states, respectively.

	$I^{(5)}$	$I^{(7)}$	$I^{(9)}$	$I^{(2n+1)}$
T_1	coh.¬	coh.¬	coh.¬	coh.
T_2	pop.→coh.¬	pop.¬	pop.¬	pop.
T_3	*¬	coh.→coh.¬	coh.¬	coh.
T_4	*	*	pop.→coh.¬	pop.
⋮	⋮	⋮	⋮	⋮
T_n	*	*	*	$\begin{cases}\text{coh.}(n=\text{odd})\\ \text{pop.}(n=\text{even})\end{cases}\rightarrow\text{coh.}$

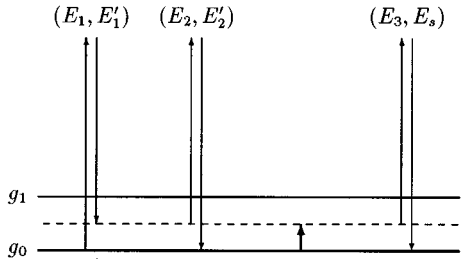

FIG. 5. Different expression of the fifth-order diagram given in Fig. 4. The lower solid line implies the g_0 state while the upper the g_1 state. The broken line stands for the vibrational coherence state. The time runs from the left to the right.

Let us examine the first diagram in Fig. 4, which is one representative diagram of $I^{(5)}$. First, notice that the distance between the leftmost and the middle black circles is T_1, and that between the middle and the rightmost is T_2. Then we realize that the system is in the vibrational coherence state in the period T_1, while in the T_2 period the system goes from the population to the coherence at the time of anharmonic interaction denoted by the cross. The above statement is true of all of the diagrams, in which the cross (anharmonic interaction) is on the T_2 segment.

States for the each period are summarized in Table I. Except for the last period T_n, the odd time periods detect the dephasing processes while the even time periods detect the population relaxation. The last period T_n for even-n describes both the dephasing and the population, while that for odd-n describes only the dephasing process.

From the above discussions we can make the following statements. First, since the T_1 period describes the coherence relaxation (or the dephasing processes), it is natural that all the signals resemble each other when plotted as a function of T_1 if the other time periods are fixed. Second, the two-dimensional¬ signals¬ $I^{(5)}(T_1,T_2)$¬ and¬ $I^{(9)}(T_1,T_2=0, T_3=0,T_4)$ may be similar since the double-sided diagrams of $I^{(9)}(T_1,T_2=0,\ T_3=0,T_4)$ (with $T_2=T_3=0$) and $I^{(5)}(T_1,T_2)$ are essentially the same, although the origins are very different since $I^{(5)}(T_1,T_2)$ and $I^{(9)}(T_1,T_2=0,\ T_3=0,T_4)$ come from the third- and fifth-order anharmonicities, respectively. On the other hand, we can expect the two-dimensional signals $I^{(5)}(T_1,T_2)$ and $I^{(7)}(T_1,T_2=0,T_3)$ not to resemble. This is because in the last period T_2 of the diagram of $I^{(5)}(T_1,T_2)$, the system goes from the population to the coherence state (at the cross), while in the last period T_3 of $I^{(7)}(T_1,T_2=0,T_3)$ the system remains in the coherence state despite the anharmonic interaction.

For the multivibrational-level system or the oscillator in the coordinate representation (the Brownian oscillator model), the first period T_1 also detects the dephasing while the other periods $T_2,\cdots,T_n$ probe the mixture of the population relaxation and the dephasing process, and the above statements may be reasonable even in such a case.

One can express the physical pictures in another schematic way. Figure 5 shows such an example corresponding to the double-sided Feynman diagram of the fifth-order response function presented in Fig. 4. In this type of diagram the upper (lower) horizontal solid line stands for the vibrational population state $|g_1\rangle\langle g_1|(|g_0\rangle\langle g_0|)$, while the horizontal broken line implies the vibrational coherent states $|g_1\rangle\langle g_0|$ and $|g_0\rangle\langle g_1|$. Time runs horizontally from left to right. The system is initially in the ground state $|g_0\rangle\langle g_0|$ (at the left end in Fig. 5). Then the first pair of laser pulses (E_1 and E_1') brings the system to the vibrational coherence states $|g_1\rangle\langle g_0|$ and $|g_0\rangle\langle g_1|$. The second pair of pulses (E_2 and E_2') brings the system back to $|g_0\rangle\langle g_0|$. Since we take into account the anharmonic interaction after the second pair of pulses, which is denoted by the short arrow, the system can

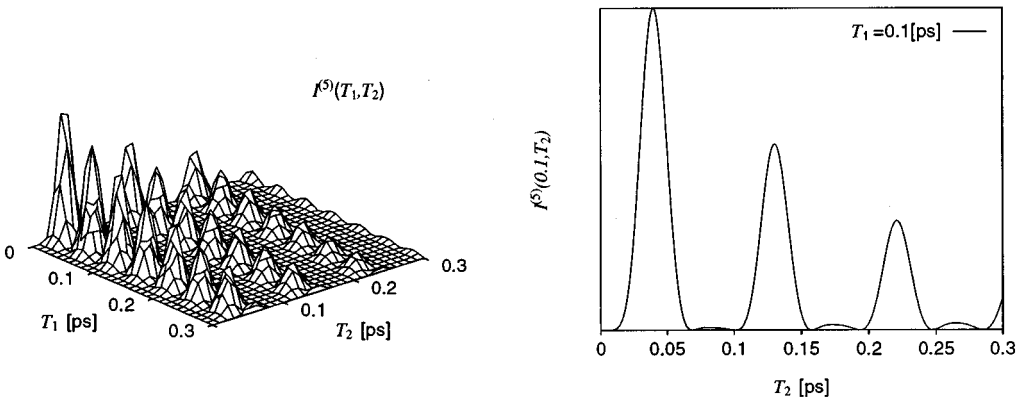

FIG. 6. Signals of the off-resonant fifth-order spectroscopy as a function of the two delay times T_1 and T_2 and of the last delay time T_2.

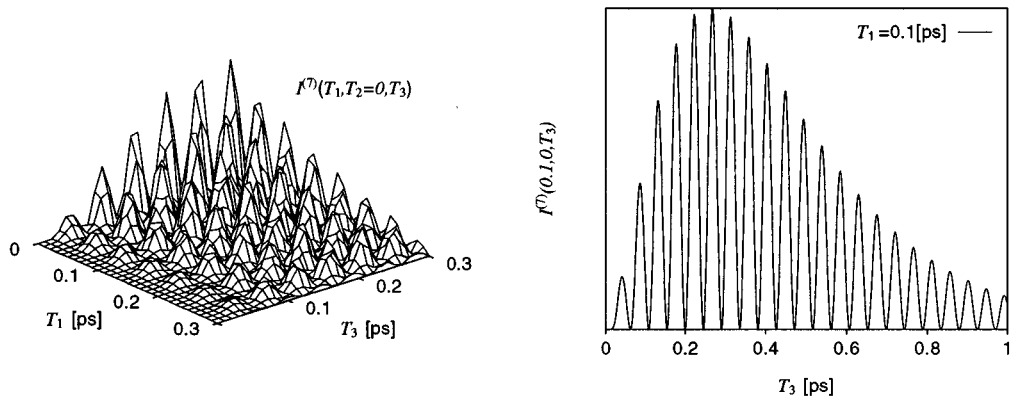

FIG. 7. Signals of the off-resonant seventh-order spectroscopy as a function of selected two delay times T_1 and T_3 and of the last delay time T_3.

change its state to the coherent one without laser interaction. Thus, the final pulse E_3 can induce the signal E_s. From this diagram, it is clear why the anharmonic interaction is essential for the system to have a signal in the fifth-order optical processes.

V. NUMERICAL SIMULATIONS

The profiles of signals expected from the physical pictures in the previous section may be summarized in the following statements:

(1) The $(2n+1)$th-order off-resonant signals $I^{(2n+1)}$ will show slow rise as a function of T_n.
(2) All profiles of $I^{(2n+1)}$ (for any integer n) as functions of the T_1 period (with the other period fixed) will be similar since the same dephasing process is probed during period T_1 for any n.
(3) All¬ of¬ the¬ two-dimensional¬ signals $I^{(5+4n)}(T_1,0,\cdots,0,T_{5+4n})$ (for any integer n) as a function of two time variables T_1 and T_{5+4n} will show similar profiles since the signals detect similar physical processes, although the origins are quite different. In the same way the 2D signals $I^{(7+4n)}(T_1,0,\cdots,0,T_{7+4n})$ may resemble each other.

In the following, we present numerical results of the analytical expressions given in Sec. III and examine the above statements. For simplicity we reduce the number of time variables by setting $T_2=0$ for the seventh order and by $T_2=T_3=0$ for the ninth order. In this configuration of pulses, the seventh- and ninth-order signals $I^{(7)}(T_1,T_2=0,T_3)$ and $I^{(9)}(T_1,T_2=0,\ T_3=0,T_4)$ reduce to two-dimensional spectroscopy.

To carry out calculations, we take the parameters from the OKE experiments on chloroform ($CHCl_3$). The vibrational modes of this substance can be described by the following three modes coupled to the Ohmic baths:[2,15]

$$\begin{aligned} &\Omega_1=39.00 \quad \gamma_1=77.0 \\ &\Omega_2=258.5 \quad \gamma_2=15.0¬ \\ &\Omega_3=368.5 \quad \gamma_3=22.0, \end{aligned} \tag{5.1}$$

where the unit of parameters is cm^{-1}. We assume that only the third mode Ω_3 has anharmonicity. The results for $I^{(5)}$, $I^{(7)}$, and $I^{(9)}$ are shown in Figs. 6–8. The features of the signals can be summarized in the following way.

T_1 *dependence*: If the last period T_n is fixed ($n=2$, 3, and 4 for $I^{(5)}$, $I^{(7)}$, and $I^{(9)}$, respectively), all the signals $I^{(5)}$–$I^{(9)}$ oscillates with the frequency $2\Omega_3$ along the T_1

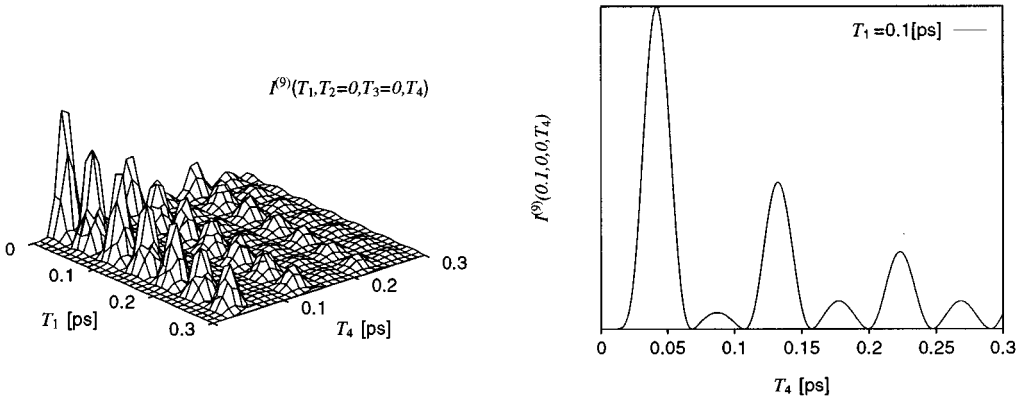

FIG. 8. Signals of the off-resonant ninth-order spectroscopy as a function of selected two delay times T_1 and T_4 and of the last delay time T_4.

axis. The envelopes of all the signals are monotonously decreasing with time. At $T_1=0$, envelopes may take a nonzero value.

T_n *dependence*: If T_1 is fixed, the signals $I^{(5)}$ and $I^{(9)}$ vibrate with frequency Ω_3 along the T_n axis while $I^{(7)}$ with $2\Omega_3$. The envelopes of $I^{(5)}$ and $I^{(9)}$ are monotonously decreasing with time, while that of $I^{(7)}$ peaks at around $T_3=0.25$. Around $T_1=0$, all of the envelopes slowly rise from zero.

The reason the oscillations in the signals appear at the frequency Ω_3 and $2\Omega_3$ is that we assumed that only the Ω_3 mode of the chloroform has anharmonicity. The slow rise for small T_n supports the first statement (inferred from the analytical expressions). The 2D signals in Figs. 6–8 exhibit oscillation with the same frequency $2\Omega_3$ in T_1, which supports our second statement (discussed from the double-sided diagrams). The fact that the whole 2D profiles of $I^{(5)}$ and $I^{(9)}$ are similar, while they look rather different from the 2D profile of $I^{(7)}$, confirms the third statement. The behavior of the envelopes of the signal can be explained in the following way. First of all, since T_1 and T_n periods both contain the dephasing processes (see Fig. 4), the longer these periods are, the weaker the strength of oscillations become: this is why all the envelopes decrease with time. The envelope of the $I^{(7)}$ signal with fixed T_1, however, has a peak. This is because we have the double-sided diagram in which the T_3 period is rephased during the T_1 period. In those types of the diagram, the T_1 period is in the state $|g_1\rangle\langle g_0|$ while the T_3 period is in $|g_0\rangle\langle g_1|$, or vice versa. One of these diagrams can be obtained by changing the diagram for $R^{(7)}$ in Fig. 4 by lowering the rightmost and the second rightmost black circles (laser interactions). These diagrams are the origin of the Raman-echo signal in appropriate models.[5] In this model, however, we cannot single out these type of diagrams by the phase matching condition. The remnant of this echolike effect may be observed as a peak of the T_3 envelope of $I^{(7)}$.

VI. DISCUSSIONS

We presented the three-step Feynman rule for the nonequilibrium expectation or the multicorrelation functions. The higher-order off-resonant signals were calculated in a compact analytical form by the rule. The physical picture for the signals was given with the help of the double-sided Feynman diagrams. We carried out the numerical calculations of the analytical expressions using the parameters obtained from the experiment, and compared the results with physical pictures obtained from the double-sided Feynman diagrams.

In this paper, we employ the linear polarization approximation $\alpha=\alpha_0+\alpha_1 q$ for simplicity. If we take into account the higher-order terms, i.e., $\alpha_2 q^2+\alpha_3 q^3+\cdots$, the profile of the signal will be governed by the relative importance of them and the anharmonicity. Such a consideration has already been done[15] in the case of the fifth-order signal, and it is also possible to include the nonlinearity of the polarizability for the higher-order signals by using the three-step Feynman diagram method.

In this article we concentrated on off-resonant measurements using optical pulses. Corresponding experiments are also possible by using infrared pulses to probe the vibrational transitions.[24] In this case signals originate from the electric dipole. Our theory can be used to study the case by replacing $\hat{P}$ with the transition dipole moment μ. In this type of experiment, we measure the correlation function of $\mu(t)$ instead of $\alpha(t)$. Both experiments are complementary.

ACKNOWLEDGMENTS

The authors greatly acknowledge K. Tominaga and K. Yoshihara for fruitful discussions. Financial support for this work was partially provided by Grand-in-Aid for Scientific Research from the Japan Ministry of Education, Science, Sports, and Culture.

APPENDIX A: THE THREE-STEP FEYNMAN RULE

In this Appendix, we present the three-step rule explicitly by clarifying the definitions of the *simplified diagrams* and *specified diagrams* with some examples. Derivation can be done from Eq. (B28).

We represent the *simplified* Feynman diagrams proportional to

$$\prod_{i=1}^{n+1} \alpha_{k_i} \cdot \prod_{j=3} g_j^{l_j} (k_i=1,2,\cdots;\ l_j=0,1,2,\cdots)$$

in the following manner. Here, l_j corresponds to the order in the jth-order anharmonicity $g_j q^j$.

A. Rules for simplified diagrams

A1. Prepare $n+1$ white circles corresponding to $\alpha_{k_1},\alpha_{k_2},\cdots,\alpha_{k_{n+1}}$. The white circle corresponding to α_i from which i lines emerge shall be called the ith-order external point.

A2. Prepare l_j black circles $(j>3)$ corresponding to the jth-order anharmonicity $V_j(q)$. The black circle corresponding to $V_j(q)$ from which j lines go out shall be called the jth-order internal point. Note here that the total number of internal points (or the black circles) in the diagram is $v=l_3+l_4+\cdots$. The internal points are also called *vertices*.

A3. Draw all possible connected diagrams by linking these internal and external points by lines (propagators). A connected diagram is the one in which arbitrary two points are connected directly or indirectly through lines.

If one cannot make a connected diagram out of the external and internal points prepared in A1 and A2, it suggests that the contribution of this order is zero. By use of the simplified Feynman diagram we can single out nonzero contributions to the response functions. Analytical expressions for the simplified Feynman diagrams are given in Eq. (B28).

Each simplified Feynman diagram can be expressed by *specified* Feynman diagrams. The specified diagram is the simplified one with $(+,-,3)$ indices and time variables attached to all the internal and external points and given in the following manner.

B. Rules for specified diagrams

B1. Attach $n+1$ time variables $0, T_1, T_1+T_2, \cdots, T_1+T_2+\cdots+T_n$ to the $n+1$ external points in an arbitrary way.

B2. Attach v time variables $t_1, t_2, \cdots, t_v$ to the v internal points in an arbitrary way.

B3. Attach the ''+'' or ''−'' index to each line emerging from an external point. An odd number of ''+'' must be attached to the lines from a single external point,¬ except¬ the¬ external¬ point¬ labeled $T_1+T_2+\cdots+T_n$ in B1. To all the lines from this special external point the ''−'' indices must be attached. As a result, the ith-order external point in a diagram has $2j+1$ lines labeled ''−'' and $i-2j-1$ lines labeled ''+'', or has i lines all labeled ''−,'' where $2j+1$ stands for an odd number and j can be an any integer from zero to $(i-1)/2$.

B4. Attach the index ''3'' to all lines emerging from an internal point, or attach the index ''+'' or ''−'' to each line from an internal point. One must attach an odd number of ''+'' to the lines from a single internal point, but cannot attach ''3'' and ''+'' (''−'') at the same time to the lines from a single internal point. It follows that the ith-order internal point in a diagram has $2j+1$ lines labeled ''−'' and $i-2j-1$ lines labeled ''+,'' or has i lines all labeled ''3,'' where $2j+1$ stands for an any odd number from one to i.

Note here that the diagram which contains the following lines vanishes and thus can be excluded from the following discussions.

b1. Line whose extremities are ''+'' and ''+'' (propagators connecting ''+'' and ''+'').

b2. Line whose extremities are ''+'' and ''3.''

b3. Line whose extremities are $(-,t)$ and $(+,t')$ where $t<t'$. (The propagator connecting ''−'' and ''+'' is causal.)

It can be shown that a simplified Feynman diagram is expressed as the sum of all possible specified diagrams obtained by the above rule which are topologically distinct from each other. Namely, we have

$$\text{A simplified diagram } \Gamma = \sum \text{ [topologically distinct specified diagrams derived from the simplified diagram } \Gamma\text{].} \tag{A1}$$

The analytical expression for a specified Feynman diagram is obtained from Eq. (B28) as follows.

C. Rules for analytical expressions

C1. Associate $\alpha_i/4^j$ with the ith-order external point which has $2j+1$ number of lines labeled ''+'' and (remaining) $i-2j-1$ number of lines labeled ''−.''

C2. Associate α_i with the ith-order external point which carries the time variable $T_1+T_2+\cdots+T_n$ and whose i lines are all labeled ''−.''

C3. Associate $-ig_k/(4^j\hbar)$ with the kth-order internal point which has $2j+1$ number of lines labeled ''+'' and (remaining) $k-2j-1$ number of lines labeled ''−.''

C4. Associate $-g_i/\hbar$ with the ith-order internal point whose i lines are all labeled ''3.''

C5. Associate the propagator $D^{(lm)}(t,t')$ $[l,m=+,-,3]$ to a line whose extremities are named (l,t) and (m,t').

C6. Integrate the product of all factors described in the above over the internal time variables $t_1, t_2, \cdots, t_v$. The range of integration for an internal point whose lines are all labeled ''3'' is from 0 to $\beta\hbar$. All the other internal points are integrated from 0 to ∞.

C7. The contribution of the diagram is obtained by the quantity obtained in C6 multiplied by $(i/\hbar)^n/S$, where the symmetry number S is the product of the line symmetry number S_L and the vertex one S_V of the diagram.

To help understand the above rules, we present several examples. First, consider the two-time response function:

$$\begin{aligned} R^{(3)}(T_1) = {} & \frac{i}{\hbar}\,\alpha_1^2\langle[q(T_1),q(0)]\rangle \\ & + \frac{i}{\hbar}\,\alpha_1\alpha_2\langle[q^2(T_1),q(0)]+[q(T_1),q^2(0)]\rangle \\ & + \frac{i}{\hbar}\,\alpha_2^2\langle[q^2(T_1),q^2(0)]\rangle+\cdots.\neg \end{aligned} \tag{A2}$$

Following rule A, the term proportional to α_1^2 is readily given by the simplified diagrams

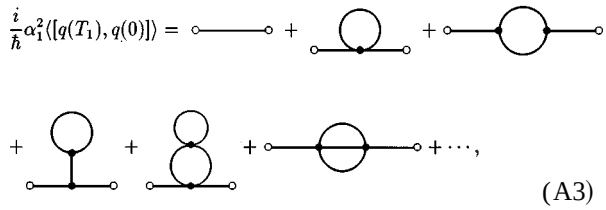

(A3)

where we consider the g_3 and g_4 anharmonicities explicitly and draw up to the second order in these anharmonicities.

By applying rule B, the above simplified diagrams can be translated into the specified diagrams

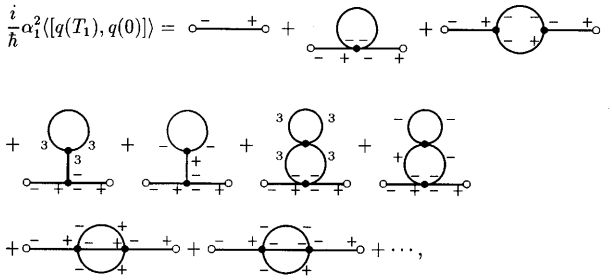

(A4)

where all the time indices are omitted. Then analytical expressions are readily obtained from rule C. For instance,

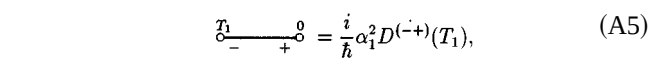

$$= \frac{i}{\hbar}\alpha_1^2 D^{(-+)}(T_1), \tag{A5}$$

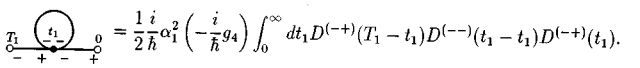

$$= \frac{1}{2}\frac{i}{\hbar}\alpha_1^2\left(-\frac{i}{\hbar}g_4\right)\int_0^\infty dt_1 D^{(-+)}(T_1-t_1)D^{(--)}(t_1-t_1)D^{(-+)}(t_1). \tag{A6}$$

Note the line symmetry factor S_L is 2 in Eq. (A6).

Second, consider the two-time response function:

$$R^{(5)}(T_1,T_2)=\left(\frac{i}{\hbar}\right)^2\alpha_1^3\langle[[q(T_1+T_2),q(T_1)],q(0)]\rangle + \left(\frac{i}{\hbar}\right)^2\alpha_1^2\alpha_2\langle[[q^2(T_1+T_2), q(T_1)],q(0)]+2 \text{ terms}\rangle+\cdots .\neg \tag{A7}$$

By use of rules A and B, the terms proportional to $\alpha_1^2\alpha_2$ are written down as

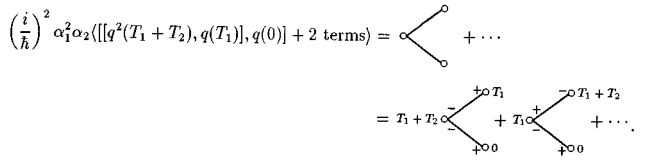

$$\left(\frac{i}{\hbar}\right)^2\alpha_1^2\alpha_2\langle[[q^2(T_1+T_2),q(T_1)],q(0)]+2 \text{ terms}\rangle = \cdots$$

$$= T_1+T_2 + T_1 + \cdots . \tag{A8}$$

Third, we consider the three-time response function $R^{(7)}(T_1,T_2,T_3)$. Following rule A, the simplified diagrams are given as

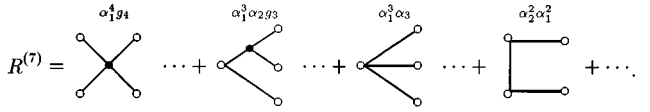

$$R^{(7)} = \alpha_1^4 g_4 \cdots + \alpha_1^3\alpha_2 g_3 \cdots + \alpha_1^3\alpha_3 \cdots + \alpha_2^2\alpha_1^2 + \cdots . \tag{A9}$$

Here, the labels above each diagram show the order of the diagram.

APPENDIX B: ANALYTICAL EXPRESSION FOR THE SIMPLIFIED DIAGRAM

By introducing the nonequilibrium generating functional $W(J)$, we obtained Eq. (A6) of our previous paper[15]:

$$R^{(5)}(T_1,T_2)=\left(\frac{i}{\hbar}\right)^2[\overline{\alpha}(\partial_1(0))\overline{\alpha}(\partial_1(T_1))-\overline{\alpha}(\partial_1(0)) \times\overline{\alpha}(\partial_2(T_1))-\overline{\alpha}(\partial_2(0))\overline{\alpha}(\partial_1(T_1)) +\overline{\alpha}(\partial_2(0))\overline{\alpha}(\partial_2(T_1))] \times\overline{\alpha}(\partial^{(-)}(T_1+T_2))\,\frac{i}{\hbar}\,W(J)\big|_{J=0},\neg \tag{B1}$$

where

$$\overline{\alpha}(\partial(t))=\alpha_0+\alpha_1\partial(t)+\frac{\alpha_2}{2!}[\partial(t)]^2+\cdots .\neg \tag{B2}$$

Introducing the sign factor

$$\mathrm{sgn}_{\{i_n\}}=(-1)^{i_1+i_2+\cdots+i_n-n},\neg \tag{B3}$$

and the time variables

$$\begin{aligned} s_1&=0,\\ s_2&=T_1,\\ s_3&=T_1+T_2,\\ &\vdots\\ s_{n+1}&=T_1+T_2+\cdots+T_n,\neg \end{aligned} \tag{B4}$$

we can generalize the above expression to the form

$$R^{(2n+1)}(T_1,T_2,\cdots,T_n) =\left(\frac{i}{\hbar}\right)^n\sum_{i_1=1}^{2}\sum_{i_2=1}^{2}\cdots\sum_{i_n=1}^{2}\mathrm{sgn}_{\{i_n\}}\,\overline{\alpha}(\partial_{i_1}(s_1)) \times\overline{\alpha}(\partial_{i_2}(s_2))\cdots\overline{\alpha}(\partial_{i_n}(s_n))\overline{\alpha}(\partial^{(-)}(s_{n+1}))\,\frac{i}{\hbar}\,W(J)\Big|_{J=0}. \tag{B5}$$

By expanding the polarizability $\overline{\alpha}$ we have

$$R^{(2n+1)}(T_1,T_2,\cdots,T_n) =\left(\frac{i}{\hbar}\right)^n\sum_{j_1=1}^{\infty}\sum_{j_2=1}^{\infty}\cdots\sum_{j_{n+1}=1}^{\infty}\frac{\alpha_{j_1}}{j_1!}\frac{\alpha_{j_2}}{j_2!}\cdots\frac{\alpha_{j_{n+1}}}{j_{n+1}!} \times\sum_{i_1=1}^{2}\sum_{i_2=1}^{2}\cdots\sum_{i_n=1}^{2}\mathrm{sgn}_{\{i_n\}}\,\partial_{i_1}^{j_1}(s_1)\partial_{i_2}^{j_2}(s_2)\cdots\partial_{i_n}^{j_n}(s_n) \times[\partial^{(-)}(s_{n+1})]^{j_{n+1}}\,\frac{i}{\hbar}\,W(J)\Big|_{J=0}.\neg \tag{B6}$$

Notice here that we have dropped the contribution from $j_l=0$ since $j_l=0$ corresponds to the c-number part of the polarizability α_0 and we are considering the expectation values of multicommutator of the polarizability.

By mathematical induction with respect to n we have

$$\frac{\alpha_{j_1}}{j_1!}\frac{\alpha_{j_2}}{j_2!}\cdots\frac{\alpha_{j_n}}{j_n!}\sum_{i_1=1}^{2}\sum_{i_2=1}^{2}\cdots\sum_{i_n=1}^{2}\mathrm{sgn}_{\{i_n\}}\,\partial_{i_1}^{j_1}(s_1)\times\partial_{i_2}^{j_2}(s_2)\cdots\partial_{i_n}^{j_n}(s_n) \tag{B7}$$

$$=\alpha_{j_1}^{(+-)}(\partial(s_1))\,\alpha_{j_2}^{(+-)}(\partial(s_2))\cdots\alpha_{j_n}^{(+-)}(\partial(s_n)),\neg \tag{B8}$$

where

$$\alpha_i^{(+-)}(\partial(t))=\frac{\alpha_i}{i!}\left[\partial_1^i(t)-\partial_2^i(t)\right] \tag{B9}$$

$$=\alpha_{i\neg}\sum_{j=0}^{2j+1<i}\frac{1}{2^{2j}}\frac{[\partial^{(+)}(t)]^{2j+1}}{(2j+1)!}\times\frac{[\partial^{(-)}(t)]^{i-2j-1}}{(i-2j-1)!}.\neg \tag{B10}$$

Thus, we arrive at

$$R^{(2n+1)}(T,T_2,\cdots,T_n)=\left(\frac{i}{\hbar}\right)^n\sum_{j_1=1}^{\infty}\sum_{j_2=1}^{\infty}\cdots\sum_{j_{n+1}=1}^{\infty}\alpha_{j_1}^{(+-)}(\partial(s_1))\times\alpha_{j_2}^{(+-)}(\partial(s_2))\cdots\alpha_{j_n}^{(+-)}(\partial(s_n))\times\overline{\alpha_{j_{n+1}}}(\partial^{(-)}(s_{n+1}))\frac{i}{\hbar}\,W(J)\Big|_{J=0}.\neg \tag{B11}$$

By applying the method explained in Appendix A in Ref. 21 [see Eq. (A7) in Ref. 21], we have

$$R^{(2n+1)}(T_1,T_2,\cdots,T_n)=\left(\frac{i}{\hbar}\right)^n e^{\partial/\partial\varphi D\partial/\partial\varphi}e^{V[\varphi]}\sum_{j_1=1}^{\infty}\sum_{j_2=1}^{\infty}\cdots\times\sum_{j_{n+1}=1}^{\infty}\alpha_{j_1}^{(+-)}(\varphi(s_1))\alpha_{j_2}^{(+-)}(\varphi(s_2))\cdots\times\alpha_{j_n}^{(+-)}(\varphi(s_n))\overline{\alpha}_{j_{n+1}}(\varphi^{(-)}(s_{n+1}))\big|_{\varphi=0,\mathrm{conn}}.\neg \tag{B12}$$

As specified below, $(\partial/\partial\varphi)D(\partial/\partial\varphi)$ is the second-order derivative operator with respect to the three variables $\varphi^{(+)}$, $\varphi^{(-)}$, and φ_3, and $V[\varphi],\alpha_i^{(+-)}(\varphi(t)),\overline{\alpha_i}(\varphi^{(-)}(t))$ are polynomial function(al)s of the three variables. The operation $|_{\varphi=0}$ in Eq. (B12) implies setting $\varphi=0$ after performing the derivatives of φ. This operation corresponds to the Wick contraction and we can resort to diagrammatic technique. Only the operations corresponding to connected diagrams are kept in Eq. (B12), as implied by conn. at the end of this equation.

The derivative operator is given by

$$\frac{\partial}{\partial\varphi}D\frac{\partial}{\partial\varphi}=\int_0^\infty dt\int_0^\infty ds\,\frac{\partial}{\partial\varphi^{(-)}(t)}D^{(-+)}(t,s)\,\frac{\partial}{\partial\varphi^{(+)}(s)}+\frac{1}{2}\int_0^\infty dt\int_0^\infty ds\,\frac{\partial}{\partial\varphi^{(-)}(t)}D^{(--)}(t,s)\,\frac{\partial}{\partial\varphi^{(-)}(s)}+\int_0^\infty dt\int_0^{\beta\hbar}d\tau\,\frac{\partial}{\partial\varphi^{(-)}(t)}D^{(-3)}(t,\tau)\,\frac{\partial}{\partial\varphi_3(\tau)}+\frac{1}{2}\int_0^{\beta\hbar}d\tau\int_0^{\beta\hbar}d\tau'\,\frac{\partial}{\partial\varphi_3(\tau)}D^{(33)}(\tau,\tau')\,\frac{\partial}{\partial\varphi_3(\tau')},\neg \tag{B13}$$

where the propagators $D^{(lm)}[l,m=(+,-,3)]$ are defined through the two-time correlation functions for the bilinearly coupled and harmonic system. Equation (B12) [or Eq. (B28) below] with this expression for $\partial/\partial\varphi D\partial/\partial\varphi$ is the origin of rules C5 and b1–b3. If we introduce the cumulant part of the autocorrelation function $C(t+i\tau)$

$$C(t+i\tau)=\langle q(0)q(t+i\tau)\rangle_{\mathrm{bilinear}},\neg \tag{B14}$$

where $0<\tau<\beta\hbar$. Then the propagators are expressed as follows:

$$D^{(-3)}(t,\tau)=C(t+i\tau), \tag{B15}$$

$$D^{(--)}(t,s)=S(t-s),\neg \tag{B16}$$

$$D^{(-+)}(t,s)=-2i\theta(t-s)A(t-s), \tag{B17}$$

$$D^{(33)}(\tau,\tau')=\theta(\tau-\tau')C(i\tau-i\tau')+\theta(-\tau+\tau')\times C(-i\tau+i\tau'), \tag{B18}$$

where S and A are the real and imaginary part, respectively $(C=S+iA)$. In the case of Ohmic dissipation, the correlation function is explicitly given by

$$C(t+i\tau)=-a_1e^{-\lambda_1(t+i\tau)}+a_2e^{-\lambda_2(t+i\tau)}-\Gamma(t+i\tau), \tag{B19}$$

where

$$a_j=\frac{\hbar}{4m\zeta}\left(1+\coth\frac{i\beta\lambda_j}{2}\right),\neg \tag{B20}$$

$$\Gamma(x)=\frac{\gamma}{m\beta}\sum_{n=-\infty}^{\infty}\frac{|\nu_n|e^{-|\nu_n|x}}{(\omega^2+\nu_n^2)^2-\gamma^2\nu_n^2},\neg \tag{B21}$$

with $\lambda_1=\gamma/2+i\zeta$, $\lambda_2=\gamma/2-i\zeta$, $(\zeta=\sqrt{\omega^2-\gamma^2/4})$, and $\nu_n=2\pi n/\beta\hbar$.

The polynomial of φ originating from the polarizability is given by

$$\alpha_k^{(+-)}(\varphi(t)) = \alpha_{k\neg} \sum_{j=0}^{2j+1<k} \frac{1}{4^j} \times \frac{[\varphi^{(+)}(t)]^{2j+1}}{(2j+1)!} \frac{[\varphi^{(-)}(t)]^{k-2j-1}}{(k-2j-1)!}, \tag{B22}$$

$$\overline{\alpha_i}(\varphi^{(-)}(t)) = \frac{\alpha_i}{i!}[\varphi^{(-)}(t)]^i.\neg \tag{B23}$$

From these expressions and Eq. (B12) [or Eq. (B28) below], we can understand rules B1, B3, C1, and C2 by noting the fact that each term in these polynomials $\alpha_k^{(+-)}(\varphi(t))$ or $\overline{\alpha(}\varphi^{(-)}(t))$ is the origin of an external point and the definition of time variables s_i in Eq. (B4).

The polynomial of φ corresponding to anharmonicity is expressed as

$$V[\varphi] = \sum_i V_i[\varphi], \tag{B24}$$

where

$$V_l[\varphi] = V_i^{(+-)}[\varphi] - V_i^{(3)}[\varphi]. \tag{B25}$$

Here,

$$V_k^{(+-)}[\varphi(t)] = -\frac{g_k}{k!}\frac{i}{\hbar}\int_0^\infty dt\left[\left(\frac{\varphi^{(+)}(t)}{2}+\varphi^{(-)}(t)\right)^k - \left(-\frac{\varphi^{(+)}(t)}{2}+\varphi^{(-)}(t)\right)^k\right]$$
$$= -\frac{i}{\hbar} g_k \int_0^\infty dt \sum_{j=0}^{2j+1<k} \frac{1}{4^j}\frac{[\varphi^{(+)}(t)]^{2j+1}}{(2j+1)!} \times \frac{[\varphi^{(-)}(t)]^{k-2j-1}}{(k-2j-1)!},\neg \tag{B26}$$

and

$$V_k^{(3)}[\varphi(t)] = -\frac{g_k}{k!}\frac{1}{\hbar}\int_0^{\beta\hbar} dt[\varphi_3(t)]^k.\neg \tag{B27}$$

We can understand rule B2, B4, C3, C4, and C6 from these expressions for V with Eq. (B12) or Eq. (B28) below by noting the fact that each term in these polynomials $V_k^{(+-)}[\varphi(t)]$ or $V_k^{(3)}[\varphi(t)]$ is the origin of an internal point.

We thus obtain the expression for the simplified diagram (contribution to the response function) proportional to

$$\prod_{i=1}^{n+1} \alpha_{k_i} \cdot \prod_{j=3} g_j^{l_j}$$

in the following form

$$\left(\frac{i}{\hbar}\right)^n e^{(\partial/\partial\varphi)D(\partial/\partial\varphi)} \prod_{j=3} (V_j[\varphi])^{l_j} \sum_{\{k_{n+1}\}} \alpha_{k_1}^{(+-)}(\varphi(s_1)) \times \alpha_{k_2}^{(+-)}(\varphi(s_2))\cdots\alpha_{k_n}^{(+-)}(\varphi(s_n)) \times \overline{\alpha}_{k_{n+1}}(\varphi^{(-)}(s_{n+1}))|_{\varphi=0,\text{conn.}},\neg \tag{B28}$$

from which Rules A, B, and C can be derived. Here, the summation $\Sigma_{\{k_n+1\}}$ implies the summation over all possible permutation of $k_1, k_2, \cdots, k_{n+1}$.

APPENDIX C: THE DOUBLE-SIDED FEYNMAN DIAGRAM

We give the rules to draw double-sided diagrams for the response functions to clarify our notations.

D. Rules for double-sided diagrams

D1. Prepare the ladder (diagram) with $(n+1)$ steps. The separation of the steps are $T_1, T_2, \cdots, T_n$ (Fig. 3). The upper solid line stands for the time evolution of ket (C_1 path) and the lower one for that of bra (C_2 path).

D2. Place a black circle at either the upper or lower end of each steps. This corresponds to the laser interaction $\alpha_1 E^2(t) q$, and absorbs or emits one quantum (a or $a^\dagger$). Here, a and $a^\dagger$ stand for the creation and annihilation operator of the vibrational mode $[q \propto (a + a^\dagger)]$.

D3. Place a single cross on either the upper or lower solid line (body of the ladder). This stands for the anharmonic interaction $g_{n+1} q^{n+1}$ and absorbs or emits quanta where the number of quanta goes in or out per one interaction can be an any number from zero [corresponding to $a^{(n+1)/2}(a^\dagger)^{(n+1)/2}$, etc.] to $n+1$ [$(a^\dagger)^{n+1}$, etc.].

[1] D. McMorrow, W. J. Lotshaw, and G. A. Kenny-Wallace, IEEE J. Quantum Electron. **24**, 443 (1988); C. Kalpouzos, D. McMorrow, W. J. Lotshaw, and G. A. Kenny-Wallace, Chem. Phys. Lett. **150**, 138 (1988); T. Hattori and T. Kobayashi, J. Chem. Phys. **94**, 3332 (1991); K. Wynne, C. Galli, and R. M. Hochstrasser, Chem. Phys. Lett. **193**, 17 (1992); Y. J. Chang and E. W. Castner, Jr., J. Chem. Phys. **99**, 113, 7289 (1993); S. Palese. L. Schilling, R. J. Dwayne Miller, P. R. Staver, and W. T. Lotshaw, J. Phys. Chem. **98**, 6308 (1994); H. P. Deuel, P. Cong, and J. D. Simon, *ibid.* **98**, 12600 (1994).

[2] M. Cho, M. Du, N. F. Scherer, G. R. Fleming, and S. Mukamel, J. Phys. Chem. **99**, 2410 (1993).

[3] Y.-X. Yan, L.-T. Cheng, and K. A. Nelson, ''Impulsive stimulated light scattering,'' in *Advances in Non-linear Spectroscopy*, edited by R. J. H. Clark and R. E. Hester (Wiley, New York, 1987), p. 299; S. Ruhman, B. Kohler, A. G. Joly, and K. A. Nelson, IEEE Quantum Electron. **24**, 470 (1988); S. Ruhman and K. A. Nelson, J. Chem. Phys. **94**, 859 (1991); B. Kohler and K. A. Nelson, J. Phys. Chem. **96**, 6532 (1992); J. Etchepare, G. Grillon, J. P. Chambaret, G. Hamoniaux, and A. Orszag, Opt. Comm. **63**, 329 (1987); P. Vöhringer and N. F. Scherer, J. Phys. Chem. **99**, 2684 (1995); Y. J. Chang, P. Cong, and J. D. Simon, *ibid.* **99**, 7857 (1995).

[4] R. Loring and S. Mukamel, J. Chem. Phys. **83**, 2116 (1985).

[5] K. Wynne, M. Müller, D. Brandt, and J. D. W. Van Voorst, Chem. Phys. **125**, 211 (1988); M. Müller, K. Wynne, and J. D. W. Van Voorst, *ibid.* **125**, 225 (1988).

[6] D. Vanden Bout, L. J. Muller, and M. Berg, Phys. Rev. Lett. **67**, 3700 (1991); L. J. Muller, D. Vanden Bout, and M. Berg, J. Chem. Phys. **99**, 810 (1993); D. Vanden Bout, L. J. Muller, J. Freitas and M. Berg, in *Ultrafast Phenomena IX*, edited by P. F. Barbara, W. H. Knox, G. A. Mourou, and A. H. Zewail (Springer-Verlag, Berlin, 1994); D. Vanden Bout, J. E. Freitas, and M. Berg, Chem. Phys. Lett. **229**, 87 (1994).

[7] R. Inaba, K. Tominaga, M. Tasumi, K. A. Nelson, and K. Yoshihara, Chem. Phys. Lett. **211**, 183 (1993); K. Yoshihara, R. Inaba, H. Okamoto, M. Tasumi, K. Tominaga, and K. A. Nelson, in *Femtosecond Reaction Dynamics*, edited by D. R. Wiersma (North-Holland, Amsterdam, 1994); K. Tominaga, R. Inaba, T. J. Kang, Y. Naitoh, K. A. Nelson, M. Tasumi, and K. Yoshihara, in *Proceedings of the XIV International Conference on*

Raman Spectroscopy, edited by N.-T. Yu and X.-Y. Li (Wiley, New York, 1994).
[8] Y. Tanimura and S. Mukamel, J. Chem. Phys. **99**, 9496 (1993).
[9] K. Tominaga, Y. Naitoh, T. J. Kang, and K. Yoshihara, in *Ultrafast Phenomena IX*, edited by P. F. Barbara, W. H. Knox, G. A. Mourou, and A. H. Zewail (Springer-Verlag, Berlin, 1994); K. Tominaga and K. Yoshihara, Phys. Rev. Lett. **74**, 3061 (1995); K. Tominaga, G. P. Keogh, Y. Naitoh, and K. Yoshihara, J. Raman Spec. **26**, 495 (1995); K. Tominaga, G. P. Keogh, and K. Yoshihara, J. Molec. Liq. **65/66**, 389 (1995); K. Tominaga and K. Yoshihara, J. Chem. Phys. **104**, 1159 (1996); K. Tominaga and K. Yoshihara, J. Chem. Phys. **104**, 4419 (1996).
[10] T. Steffen and K. Duppen, Phys. Rev. Lett. **76**, 1224 (1996); T. Steffen and K. Duppen in *Femtochemistry*, edited by M. Chergui (World Scientific, Singapore, 1995), p. 583; T. Steffen and K. Duppen, in *Ultrafast Phenomena*, Vol. 8, 1996 OSA Technical Digest Series (Optical Society of America, Washington DC, 1996), p. 208; T. Steffen, J. T. Fourkas, and K. Duppen, J. Chem. Phys. **105**, 7364 (1996); T. Steffen and K. Duppen, J. Chem. Phys. (to be published).
[11] J. A. Leegwater and S. Mukamel, J. Chem. Phys. **102**, 2365 (1995).
[12] V. Khidekel and S. Mukamel, Chem. Phys. Lett. **240**, 304 (1995).
[13] S. P. Palese, J. T. Buontempo, L. Schilling, W. T. Lotshaw, Y. Tanimura, S. Mukamel, and R. J. D. Miller, J. Phys. Chem. **98**, 12466 (1994).
[14] A. Tokmakoff, J. Chem. Phys. **105**, 1 (1996); *ibid*. **105**, 13 (1996); A. Tokmakoff and G. R. Fleming, J. Chem. Phys. (to be published).
[15] K. Okumura and Y. Tanimura, J. Chem. Phys (submitted).
[16] Y. J. Yan and S. Mukamel, J. Chem. Phys. **94**, 997 (1991).
[17] S. Mukamel, *Principles of Nonlinear Optical Spectroscopy* (Oxford University Press, New York, 1995).
[18] K. Okumura and Y. Tanimura, Phys. Rev. E **53**, 214 (1996).
[19] I. Ohmine and H. Tanaka, Chem. Rev. **93**, 2545 (1993).
[20] For a treatment of anharmonic oscillators in the level scheme instead of the coordinate scheme, see the following: J. T. Fourkas, H. Kawashima, and K. A. Nelson, J. Chem. Phys. **103**, 4393 (1995); J. T. Fourkas, *Theory of Vibrational Echo Phenomena in Harmonic and Weakly Anharmonic Oscillators*, Seventh International Conference on Time-Resolved Vibrational Spectroscopy, edited by W. Woodruff (in press); J. T. Fourkas, Laser Phys. **5**, 656 (1995).
[21] K. Okumura and Y. Tanimura, J. Chem. Phys. **105**, 7294 (1996).
[22] In another conventional case (in high energy physics) where the vacuum expectation values are the main concern, only the real time evolution operator, $e^{-iHt/\hbar}$, or only the C_1-path is required. The propagators in this case always connect two points on C_1.
[23] Two diagrams which are the same except for the position (upper or lower) of the rightmost black circle make an identical analytical contribution to the signal.
[24] D. Zimdars, A. Tokmakoff, S. Chen, S. R. Greenfield, M. D. Fayer, T. I. Smith, and H. A. Schwettman, Phys. Rev. Lett. **70**, 2718 (1993); A. Tokmakoff and M. D. Fayer, J. Chem. Phys. **103**, 2810 (1995).